SSRG International Journal of Electrical and Electronics Engineering
ISSN: 2348-8379/ https://doi.org/10.14445/23488379/IJEEE-V11I9P114

Volume 11 Issue 9, 160-171, September 2024

Original Article

Performance Analysis of EV Drive with Battery and Support from Super-Capacitor in Motoring and Regenerative Braking Conditions

Ankush A. Deosant[1], Kishor B. Porate[2]

[1,2]*Department of Electrical Engineering, Priyadarshini College of Engineering Nagpur, India.*

[1]*Corresponding Author : ankdeo@gmail.com*

Received: 06 July 2024 Revised: 09 August 2024 Accepted: 07 September 2024 Published: 28 September 2024

Abstract - *An efficient EV drive system improves the vehicle's performance and reduces power loss in the modules. The voltage stability on the source and machine sides is vital for an EV during heavy load and high-speed conditions. With drastic variations of torque and speed in a drive cycle, the EV drive system needs to be stable and robust to these variations. In this paper, a standard battery module driving the EVs PMSM with support from the SC module is proposed. The speed controller used for the PMSM is FOC, with feedback from the machine's angular speed and stator currents. The performance of the EV drive system is analyzed using only the battery module and SC module support. CC and CV control structures are introduced in the specified model as per the requirement controlling the DC bus voltage. A comparative analysis between the two models is carried out in drive mode and regenerative braking mode, and the results are presented. The evaluation of these results includes DC bus voltage stability, PMSM stability, battery and SC performance comparisons. Validation of the better system is determined by this comparative analysis of the EV drive systems. The modelling and design of the proposed systems are implemented in MATLAB Simulink software with blocks considered from the 'Power systems' library.*

Keywords - *Constant Current (CC), Electric Vehicle (EV), Field Oriented Control (FOC), Permanent Magnet Synchronous Motor (PMSM), Super Capacitor (SC).*

1. Introduction

Increasing global temperatures are caused by several factors, including fossil fuel power generation and transportation utilization. Most of the fossil fuel (coal) thermal generating plants have been replaced with renewable sources, reducing some of the carbon emissions. Most of the carbon emissions are caused by Internal Combustion (IC) engine vehicles, which are the major cause of 40% of global warming. These IC engine vehicles need to be replaced by zero-emission vehicles which drive on storage units or renewable sources.

There is also a specific category, which is hybrid vehicles, which uses multiple sources to drive the vehicle. However, hybrid vehicles are very complex and economically not viable for utilization [1]. Another type of zero-emission vehicle is a hydrogen-fueled vehicle, which uses power from a fuel cell to drive the vehicle's motor. This hydrogen fuel vehicle is economically expensive for domestic transportation; hence, it cannot be affordable for ordinary people.

Hybrid vehicles are another option to replace IC-engine vehicles, which are a combination of both electrical power and fossil fuel power that drive the vehicle. However, the vehicle drive partly depends on the electrical power, which is used only to support the IC engine drive. Because of this support to the vehicle, the mileage increases slightly above the conventional value. The only low-cost zero-emission vehicle available is battery operated EV, which drives on power from storage modules. The storage module is a combination of multiple cells in series and parallel, forming a battery pack [2].

To increase the voltage of the battery, the number of series cells is increased, and to increase the capacity, the parallel cells are increased. Renewable power generation units or grid-connected charging stations charge this battery pack. For using the charge from the battery, driving the vehicle motor a power circuit is needed to control the machine. The most common machine used in EVs is PMSM, which has very high initial torque and is very easy to control [3].

The speed of the PMSM can be varied while keeping the torque constant. This is achieved by FOC controlling the switches of the inverter connected between the storage modules and the motor. The complete structure of the proposed EV drive system with battery pack, SC module and PMSM is presented in Figure 1.

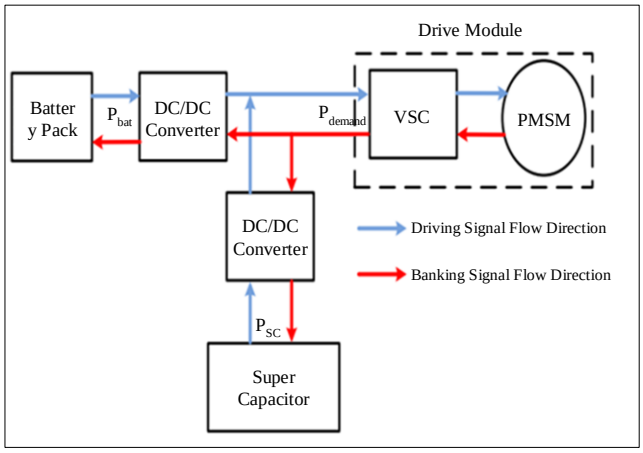

Fig. 1 Structure of the proposed EV drive system

As per the given Figure 1 the battery and SC modules are connected to the PMSM through individual DC/DC bidirectional converters [4]. A Voltage Source Converter (VSC) is connected between the PMSM and storage modules for voltage conversion (DC-AC). The battery pack provides prolonged power to the machine during the drive, and the SC provides instantaneous power during sudden changes in power demand [5].

As per the operating mode of the PMSM the DC/DC bidirectional converters and VSC will operate accordingly. During motoring mode or drive mode, the DC/DC bidirectional converters operate in boost mode or discharge mode, and VSC operates as an inverter. During regenerative braking mode, the DC/DC bidirectional converters operate in buck mode, and the VSC operates as a rectifier [6].

The voltage at the common DC bus is maintained by the controllers operating the battery and SC modules. Different controllers like CC and CV structures are proposed in this model for DC link voltage stabilization [7]. The VSC is operated by FOC controlling the speed of PMSM as per the reference given by the user. In drive mode for any given speed reference, the FOC tends to maintain the torque at a given set point [8]. During regenerative braking mode, the FOC is turned off converting the inverting operation of VSC to rectification using body diodes of the IGBT switches.

The paper is organized with an introduction to the proposed test circuit outline structure for driving an EV machine in Section 1. The different operating conditions, which include motoring and regenerative braking modes, are discussed in this Section. In Section 2, the circuit configuration is described with battery storage, SC modules and PMSM circuit topologies. The following Section 3 has the proposed control structures for the introduced circuit topologies as per the requirement of the system.

The modelling and design of all the modules are done using MATLAB software analyzing the model for better performance to the changes given in the model. The results are presented in Section 4 represented by graphical plotting with time as reference. The voltages, powers and state of charges of the modules are presented in this section, determining the better-performing circuit structure. The final Section 5 has the conclusion to the paper which finalizes the outcome of the analysis done on the proposed topology.

2. Circuit Configuration

As per Figure 1, the battery pack and SC are connected to individual DC/DC bidirectional converters with two high-frequency operating IGBTs. These converters are controlled by high-frequency switching pulse alternatively. The duty ratio of these switches is varied to change the mode of operation. These converters are operated either in boost mode or buck mode, depending on the operating condition of the EV's PMSM. Both converters have individual controllers which control the charge/discharge of the storage modules.

During discharge of the battery in boost mode as per the SOC of the SC, the operating mode of the SC bidirectional converter is changed. During sudden changes in the load demand by the PMSM, the SC provides power for a momentary time, protecting the battery. With a duty ratio of more than 50%, the bidirectional converter operates in boost mode. And when the duty ratio is below 50% the converters operate in buck mode.

In the boost mode, the converters discharge the storage units and drive the EV's PMSM. In buck mode, the converters charge the storage units from the energy generated by the PMSM during regenerative braking conditions. The power exchange between the storage modules and the PMSM is done through VSC with six switches. Each switch is a MOSFET-connected body diode combination unit to achieve bidirectional operation of VSC. The complete circuit structure of the proposed EV drive system with the mentioned converters is presented in Figure 2.

As per the given Figure 2, the battery module DC/DC converter has two MOSFET switches Q1 Q2, and the SC DC/DC converter has Q3 Q4 switches. The Q1, Q2 and Q3 Q4 switches are complementary switches which avoid short circuits. Both the inductors L1 and L2 are energy storage elements used for storing charge as per the requirement. These two converters are connected to a common DC bus which shares power to the VSC connected to PMSM. The voltage at the DC bus is to be maintained constant and stable at a certain operating limit and magnitude for the machine to operate. The DC voltage magnitude at the DC bus is maintained by the controllers included for switching pulses generation controlling the switches Q1 – Q4.

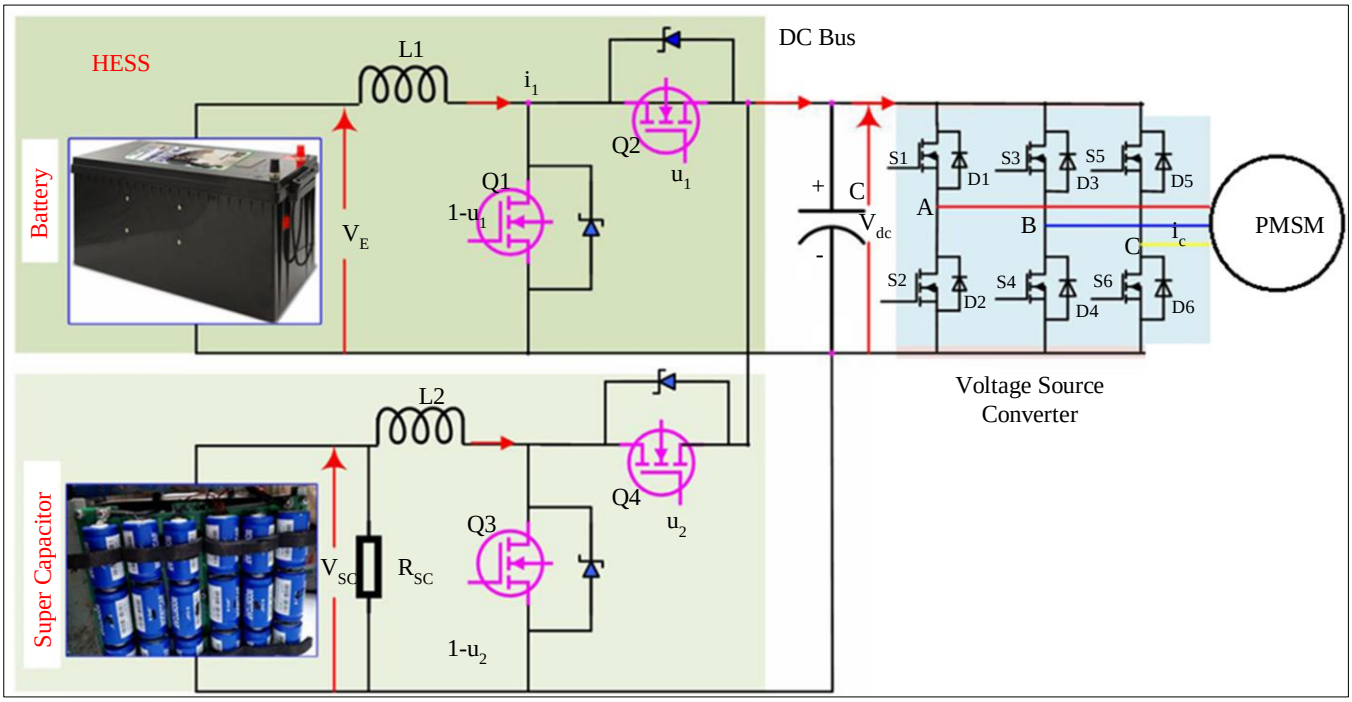

Fig. 2 Circuit structure of the proposed EV drive system

The MOSFET switches S1 – S6 are the VSC switches connected in a three-legged format for converting AC-DC or DC-AC (Inverting or Rectification) as per the operating condition. The switches S1 - S6 are given pulse from FOC in drive mode operating condition where the VSC operates as an inverter driving the PMSM. During regenerative braking conditions, the PMSM operates as a generator which needs to be equalized.

The pulses to the VSC are removed which converts the VSC to a three-phase diode bridge rectifier by the anti-parallel body diodes of the MOSFETs in the regenerative braking condition. The rectifier operating VSC now transfers power from PMSM to the DC bus which charges either the battery pack or SC unit as per the state of charge of the units. The PMSM operating mode (drive or regenerative) is changed as per the 'vehicle dynamics' generating positive or zero torque conditions. The positive torque represents the driving mode, and the zero torque represents the regenerative mode. The electromagnetic torque (T_e) of the PMSM as per the vehicle dynamics is given as:

$$T_e = Hw_r + Bw_r + F_r r i_t \quad (1)$$

Here, H is the inertia of the machine, B is the viscous friction, w_r is the rotor speed of the machine, F_r is the resistive force, r is the radius of the wheel, and i_t is the gear ratio. The Hw_r , Bw_r and i_t are the predefined variables of the machine and vehicle. w_r is measured by a speed sensor, whereas the F_r is given as:

$$F_r = mgf_r Cos\theta + \frac{1}{2}\rho_\theta C_D A_f (v + v_w)^2 + mgSin\theta \quad (2)$$

Here, m is the mass of the vehicle, g is the gravity, f_r is the rolling resistance coefficient, ρ_θ the density of air, C_D coefficient of aerodynamic drag, v is the vehicle velocity, v_w is the wind speed in the direction of vehicle drive, and θ is the ground slope angle. As per the T_e of the machine, it is determined whether the vehicle is in driving mode or in regenerative braking mode. With respect to the T_e value the switching of the FOC is done by changing the operating mode of VSC.

3. Controllers Design

The controllers for the power circuits are designed as per the operating mode of the topology. For driving the PMSM with constant torque and variable speeds FOC is adopted with signals taken from the PMSM speed sensor, stator currents and rotor angle. For constant current discharge from the battery pack during drive mode, a CC controller is implemented [9].

The CC controller needs battery voltage and current feedback signals for controlling the DC/DC converter. The CC controller generates the required duty ratio for the switches Q1 and Q2, controlling the discharge and charge current [10]. In the SC module, the DC/DC converter is controlled by the CV controller with feedback from only the DC bus voltage. This CV controller generates the duty ratio for the switches Q3 and Q4, controlling the charge and discharge of the SC.

3.1. FOC for PMSM Drive

FOC for controlling the speed of the PMSM is considered to be the most optimal controller for EV drive applications. This FOC scheme ensures that the speed of the PMSM is achieved accurately with faster settling time and reduced ripple [11]. The FOC controls the magnitude and angle of the stator winding field, which changes the speed of the rotor, maintaining the torque constant [12].

For this control, the FOC needs stator currents signals (ISabc), measured angular speed of the machine (W_{rotor}) and rotor angle position (θ_r) calculated as:

$$\theta_r = \int p \, . w_{rotor} \quad (3)$$

The complete structure of the FOC scheme for controlling the VSC in drive mode is presented in Figure 3.

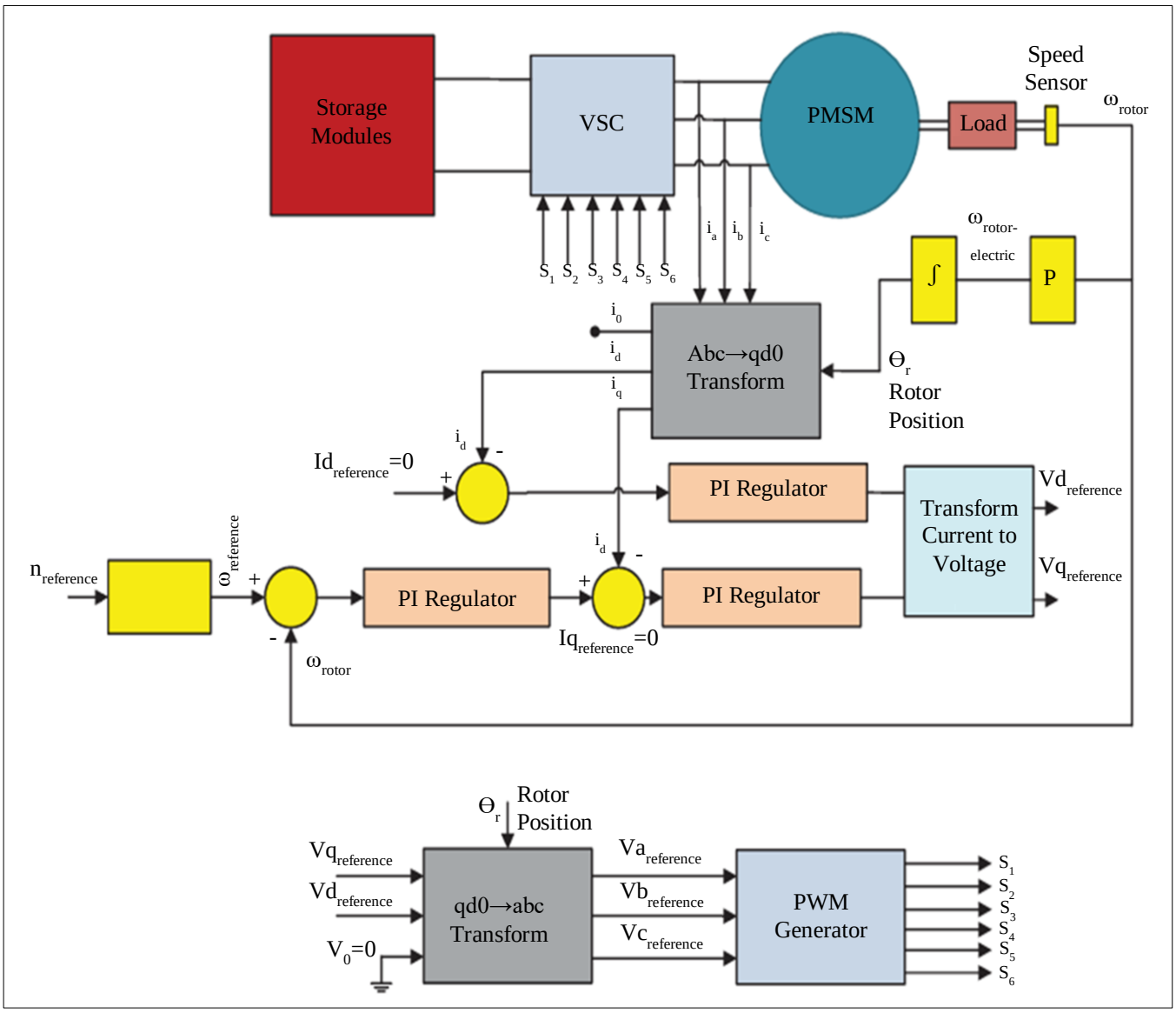

Fig. 3 FOC scheme for PMSM in drive mode

For controlling the VSC connected between the storage modules and PMSM reference Sin signals are needed for the generation of Pulse Width Modulation (PWM) pulses [13]. The Sin signals for PWM generation are derived from $Vd_{reference}$ and $Vq_{reference}$ signals expressed as:

$$Vd_{reference} = \left(Id_{reference} - i_d\right)\left(K_{pi} + \frac{K_{ii}}{s}\right) \quad (4)$$

$$Vq_{reference} = \left(Iq_{reference} - i_q\right)\left(K_{pi} + \frac{K_{ii}}{s}\right) \quad (5)$$

In the given equations, i_d i_q are the measured dq stator current components determined by Park's transformation using rotor angle position θ_r expressed as:

$$\begin{bmatrix} i_d \\ i_q \end{bmatrix} = \begin{bmatrix} Sin\ \theta_r & -Cos\ \theta_r & 0 \\ Cos\ \theta_r & Sin\ \theta_r & 0 \end{bmatrix} \begin{bmatrix} i_a \\ i_b \\ i_c \end{bmatrix} \quad (6)$$

K_{pi} K_{ii} are the proportional and integral gains of the current PI regulator. $Id_{reference}$ and $Iq_{reference}$ are the reference dq components where $Id_{reference}$ is taken as 0, and $Iq_{reference}$ is given as:

$$Iq_{reference} = (w_{reference} - w_{rotor}) \left(K_{ps} + \frac{K_{is}}{s}\right) \quad (7)$$

Here, $w_{reference}$ is the reference angular speed defined by the user as per requirement, w_{rotor} is the measured rotor angular speed, K_{ps} K_{is} are the proportional integral gains of the speed PI regulator [14, 15]. From the Vdreference and Vqreference reference dq components the Sin signals (Va* Vb* Vc*) are generated by the below inverse Park's transformation relation.

$$\begin{bmatrix} V_a^* \\ V_b^* \\ V_c^* \end{bmatrix} = \begin{bmatrix} Sin\ \theta_r & Cos\ \theta_r \\ Sin\left(\theta_r - \frac{2\pi}{3}\right) & Cos\left(\theta_r - \frac{2\pi}{3}\right) \\ Sin\left(\theta_r + \frac{2\pi}{3}\right) & Cos\left(\theta_r + \frac{2\pi}{3}\right) \end{bmatrix} \cdot \begin{bmatrix} Vd_{reference} \\ Vq_{reference} \end{bmatrix} \quad (8)$$

These Va* Vb* Vc* are compared to high frequency triangular waveform producing PWM pulses for S1 – S6 switches of VSC.

3.2. CC and CV Controllers

The CC controller is generally used during fixed current charge or discharge conditions for a storage unit [16]. The storage unit integrated with the CC controller will be either receiving or delivering the reference set current value in the controller. The internal structure of the CC controller for the battery storage module is presented in Figure 4.

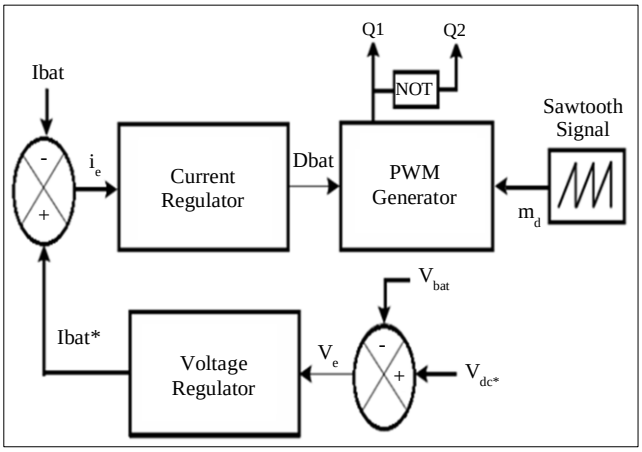

Fig. 4 CC control internal structure

As per Figure 4, the reference to the CC controller is the Vdc* value which is set as per the voltage required at the DC bus. The reference DC bus voltage Vdc* is compared to the measured battery voltage Vbat, and the error signals are given to the voltage regulator, which is generally a PI controller with tuned Kpv and Kiv values. As per the gains, the reference battery current Ibat* is generated, which is compared to the measured battery current Ibat producing error current (ie) [17]. This i_e signal is fed to the current regulator (PI) with specified gains Kpc Kic generating duty ratio (D_{bat}) for the battery module switches. The D_{bat} signal is expressed as:

$$D_{bat} = (Ibat^* - Ibat)\left(K_{pc} + \frac{K_{ic}}{s}\right) \quad (9)$$

And the Ibat* signal is expressed as:

$$Ibat^* = (Vdc^* - Vbat)\left(K_{pv} + \frac{K_{iv}}{s}\right) \quad (10)$$

The D_{bat} signal is compared to high frequency sawtooth waveform generating a pulse for switch Q1 and NOT gate signal to Q2 of the DC/DC bidirectional converter [18]. As per the reference set by the DC bus voltage, the discharging of the battery takes place running the PMSM by the battery power limiting the current discharge.

For the SC DC/DC bidirectional converter a CV controller is adopted for maintaining the DC bus voltage stable. The complete structure of the CV control internal structure is presented in Figure 5 with a single voltage regulator.

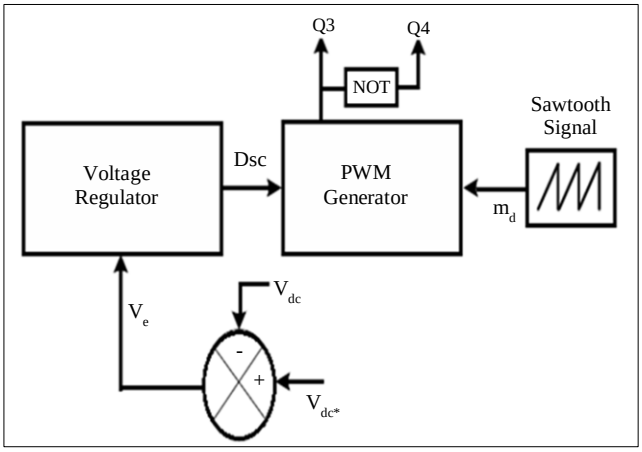

Fig. 5 CV control internal structure

As per Figure 5, the duty ratio (Dsc) for the switches Q3 and Q4 of the DC/DC bidirectional converter of the SC module is generated by a voltage regulator with input from a comparison of Vdc* and measured DC bus voltage Vdc [19]. The Dsc is expressed as:

$$D_{sc} = (Vdc^* - Vdc)\left(K_{pdc} + \frac{K_{idc}}{s}\right) \quad (11)$$

The $K_{pdc}K_{idc}$ tuned gains of the voltage regulator generate the required Dsc for the switches which maintain the DC bus voltage at the specified reference value at Vdc*. This value is set as per the required DC voltage of the PMSM which needs to be as per the rating of the machine.

3.3. FIS Controller

As the PI regulator is a conventional controller for generating the reference values or duty ratios, which have high disturbances and ripple needs to be replaced by an advanced controller. The Fuzzy Inference System (FIS) is considered to be an optimal option for replacing the PI regulator for mitigation of disturbances in the controller [20]. This reduces the ripple in the voltage and current of the module to which it is integrated. In this model, the CC controller is updated with FIS at the voltage regulator, which determines the reference battery current for running the PMSM.

The input to the FIS is the error signal generated by the comparison of Vdc* and Vbat. There are two inputs to the FIS regulator, which are named error (E) and Change in Error (CE) and one output variable (Ibat*) is required for the current regulator. Each variable consists of seven Membership Functions (MFs) defined as per the position in the range of the variable signal [21]. The variables set with MFs at specified ranges can be observed in Figure 6.

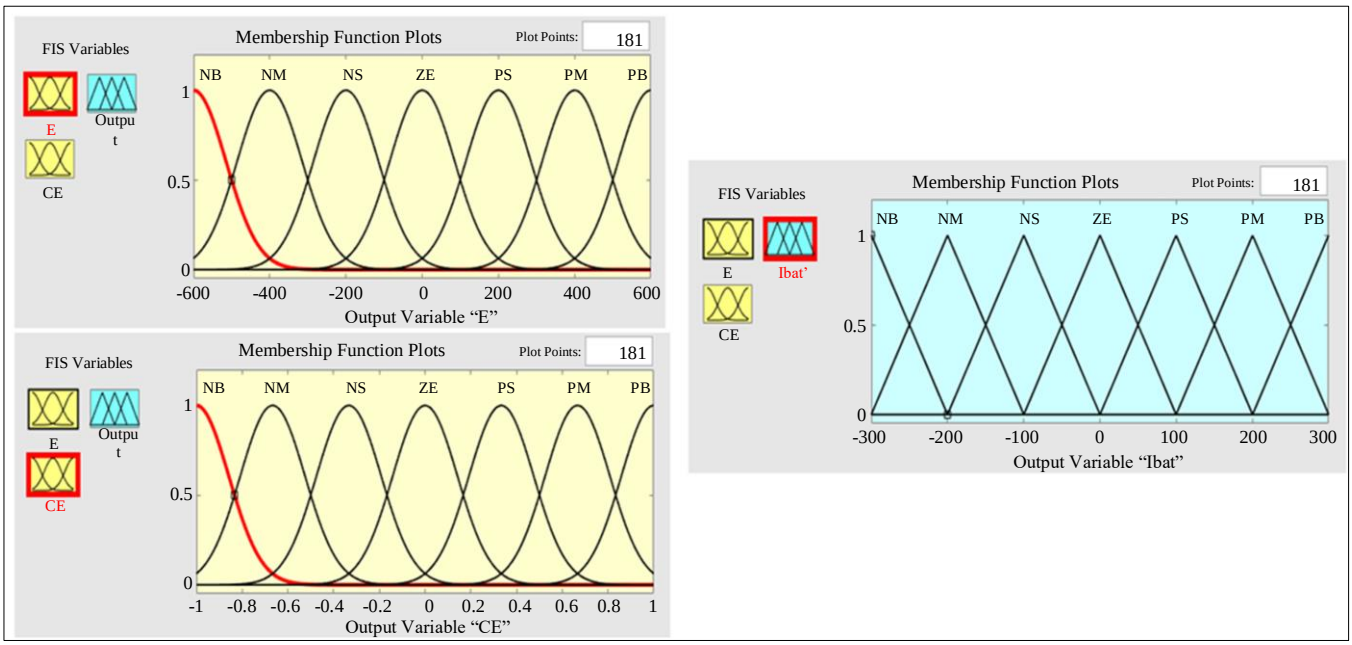

Fig. 6 MFs of input and output variables of FIS

As presented in Figure 6, all the MFs in the variables are named with the same names given as NB – Negative Big, NM – Negative Medium, NS – Negative Small, ZE – Zero, PS – Positive Small, PM – Positive Medium and PB – Positive Big [22]. The range of the E variable is set between -600 to 600 which is decided by the maximum set value at the reference.

The CE is always between -1 to 1, which is the maximum range for change in error, and the Ibat* variable is set between -300 to 300 which is tuned as per the response of the system. The output value is varied as per the range adjustment and the given rule in Table 1.

As per the given MFs range and rule table, the output value of the FIS is generated with mitigated ripple and disturbances in the signal Ibat*. This regulator is updated to the battery module, and comparative results are generated, validating the optimal control structure for the system.

Table 1. Rule table

49 Rule Base		Error (E)						
		NB	**NM**	**NS**	**ZE**	**PS**	**PM**	**PB**
Change in Error (CE)	**PB**	Z	PS	PM	PB	PB	PB	PB
	PM	NS	Z	PS	PM	PB	PB	PB
	PS	NB	NS	Z	PS	PM	PB	PB
	ZE	NB	NM	NS	Z	PS	PM	PB
	NS	NB	NB	NM	NS	Z	PS	PM
	NM	NB	NB	NB	NM	NS	Z	PS
	NB	NB	NB	NB	NB	NM	NS	Z

4. Simulation Results

The modelling and design of the drive circuit with a battery module, SC module and PMSM driven VSC circuit with all the controllers in done is Simulink environment using blocks taken from the 'Specialized Power systems' block set. All the blocks in the modeled topology are updated with specified values as given in configuration parameters Table 2.

Table 2. Topology configuration parameters

Name of the Module	Parameters
Battery	Battery pack: Lithium-Ion, Vnom = 320V, Capacity = 90Ah, SOCint = 80% DC/DC Converter: Lb = 161.95µH, Co = 220µF, fs = 5kHz CC controller: Vref = 560V, Kpv = 0.5, Kiv = 0.03, Kpc = 0.1, Kic = 0.00023
SC	Capacitance = 10F, Rdc = 8.9mΩ, Vnom = 300V, Ns = 1, Np = 1, Vint = 250V DC/DC Converter: Lb = 161.95µH, Co = 220µF, fs = 5kHz CV Controller: Vref = 560V, Kpdc = 0.1, Kidc = 0.00023
EV	PMSM: Pnom = 35kW, N = 3000rpm, Vdc = 560V, Tnom = 111Nm, Rs = 0.05Ω, Ls = 0.635mH, Φ= 0.192V.s, J = 0.011kg.m2, F = 0.001889 N.m.s, p = 4 Vehicle Dynamics: Rw=0.33, i_t=12, Mv=650, g=1.22, Crr=0.01, rho_a=5, AL=2.3, Cd=0.5 FOC: Nref = 2000rpm, ids* = 0, Kpi = 10, Kii = 0.05, Kps = 50, Kis = 2, fs = 5kHz

As per the given values in Table 2, the model block parameters are updated, and the simulation is run for

i) Battery module connected EV drive,
ii) Battery and SC modules connected EV drive with PI voltage regulator, and
iii) Battery SC modules connected to EV drive with FIS voltage regulator.

All the simulations are run with the 'power Gui' toolbox used for graph generation plotting concerning time. The measured values at each module are presented below in driving mode from 0-0.5 sec and regenerative braking mode from 0.5-1 sec.

As per Figure 7, the battery characteristics for model (i) with only the battery module operating the PMSM of the EV are presented. From 0 – 0.5 sec, the battery pack discharges with a very high current in the range of 100A and a peak value of 600 A during the initial state. This high current magnitude and peak value reduces the reliability of the battery and may lead to a dead battery pack. The PMSM characteristics for model (i) are presented in Figure 8.

As per the given reference, 2000 rpm in FOC, the speed of the PMSM is settled at 2000 rpm at 0.05 sec. To achieve the desired speed, the initial electro-magnetic torque of the machine is recorded at 110 Nm which reduces to 50 Nm at 0.05 sec as per the vehicle dynamics. For the same model (i) and operating condition, the stator currents of PMSM and mechanical torque from the vehicle dynamics are presented in Figure 9.

As observed in Figure 9, the stator currents magnitude is at 50 A during drive mode with 50Nm Tm demand, dropping near zero during regenerative braking mode when Tm becomes zero. For this condition of the model, (i) The DC link voltage is recorded to be 560V throughout the simulation of 1sec, which is represented in Figure 10.

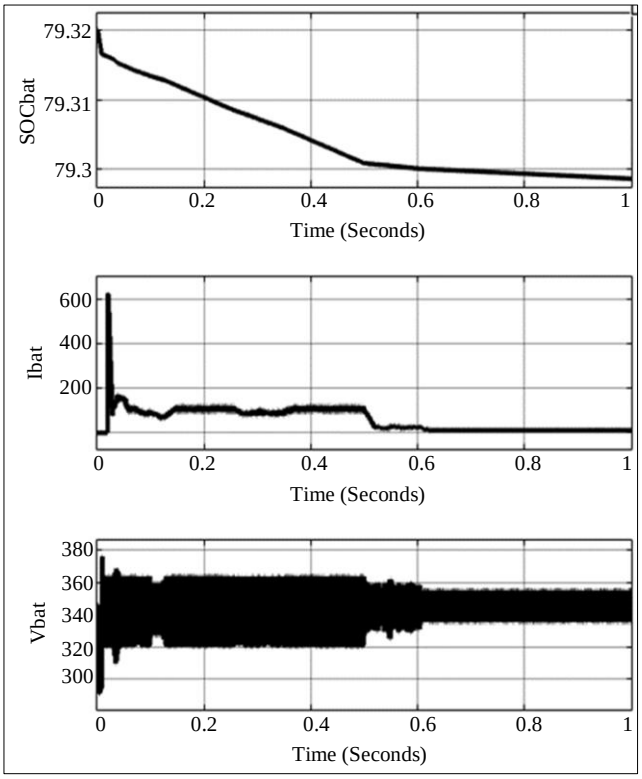

Fig. 7 Battery pack characteristics of the model (i)

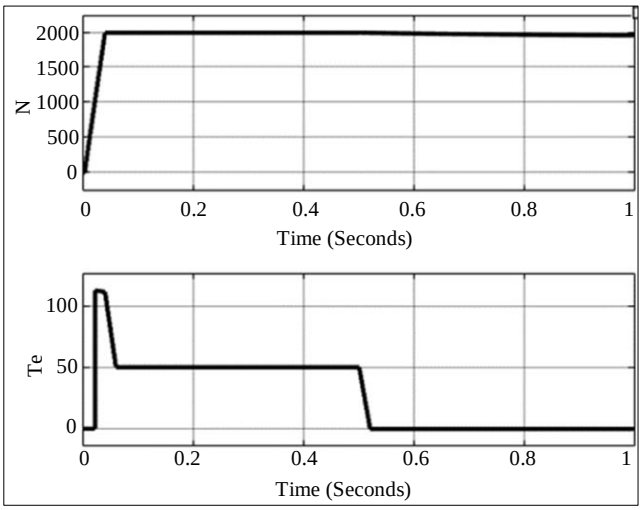

Fig. 8 PMSM speed (N) and electro-magnetic torque (Te) of the model (i)

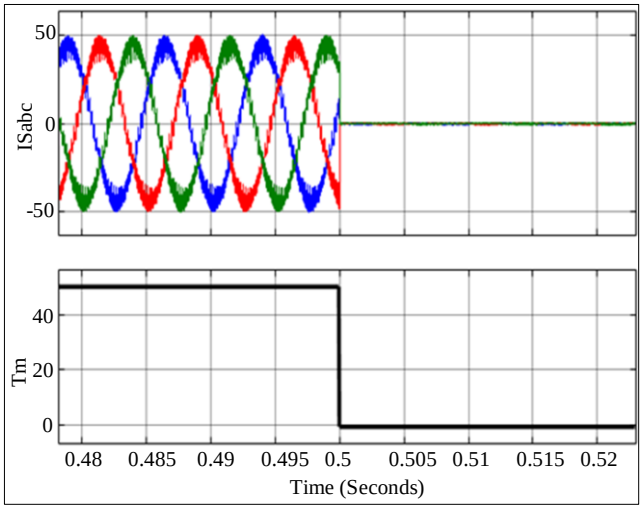

Fig. 9 Stator currents (ISabc) and mechanical torque (Tm) of PMSM of the model (i)

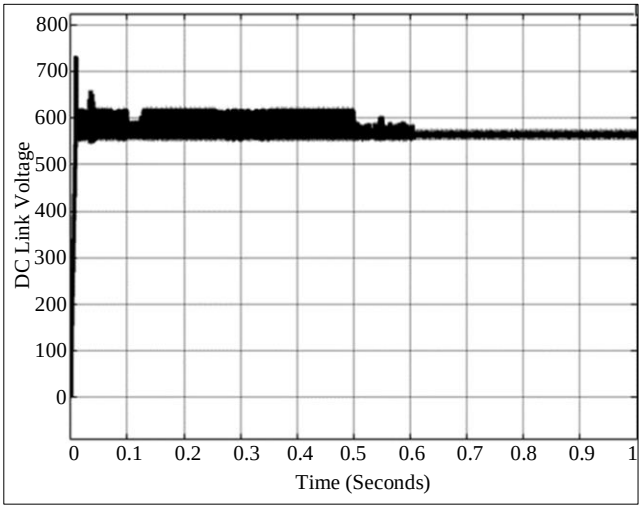

Fig. 10 DC bus voltage for model (i)

As per model (ii) the source side is updated with the SC module connected in parallel to the battery module supporting the battery pack. For the same operating conditions of driving and regenerative braking, the simulation is run with graphs generated as presented below. Figure 11 represents the battery characteristics for model (ii).

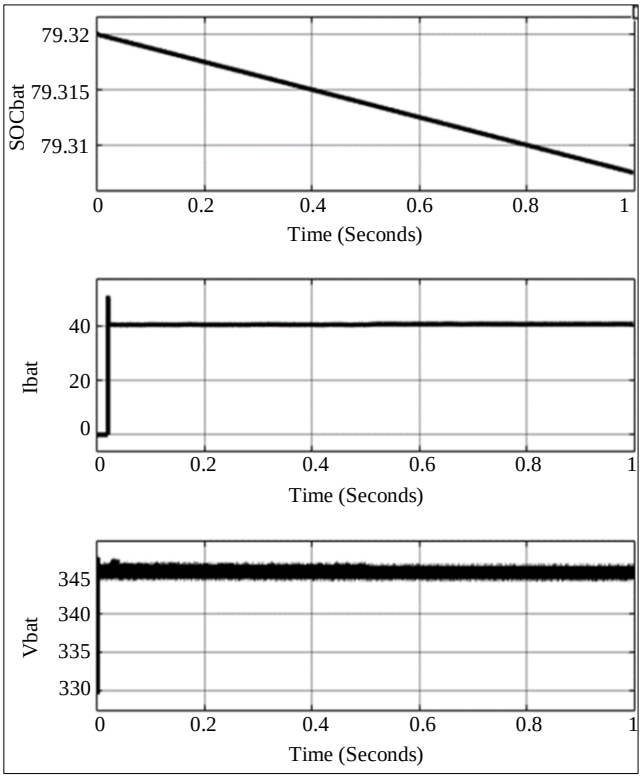

Fig. 11 Battery characteristics for model (ii)

As observed in Figure 11, the initial peak current is very low at 50 A for model (ii) as the SC provides the starting current for the PMSM. The CC controller also sets the current magnitude of the battery pack 40A and remains the same in any operating mode. As per the characteristics of SC in Figure 12, the initial current of SC is high and later settles to zero, which represents no exchange of power.

At 0.5 sec, when the regenerative braking mode is activated, the SC charges with a very high current of 50 A, sharing 40 A from the battery and 10 A from PMSM. The DC bus voltage for model (ii) is presented in Figure 13, which shows the magnitude maintained at 560 V as per the reference value set in the CV controller of the SC module.

The ISabc and Tm for model (ii) are presented in Figure 14, which are the same as in model (i), as the machine and vehicle dynamics remain the same. The N and Te of the PMSM also remain the same for model (ii), which has 2000 rpm and 50 Nm in drive mode shown in Figure 15.

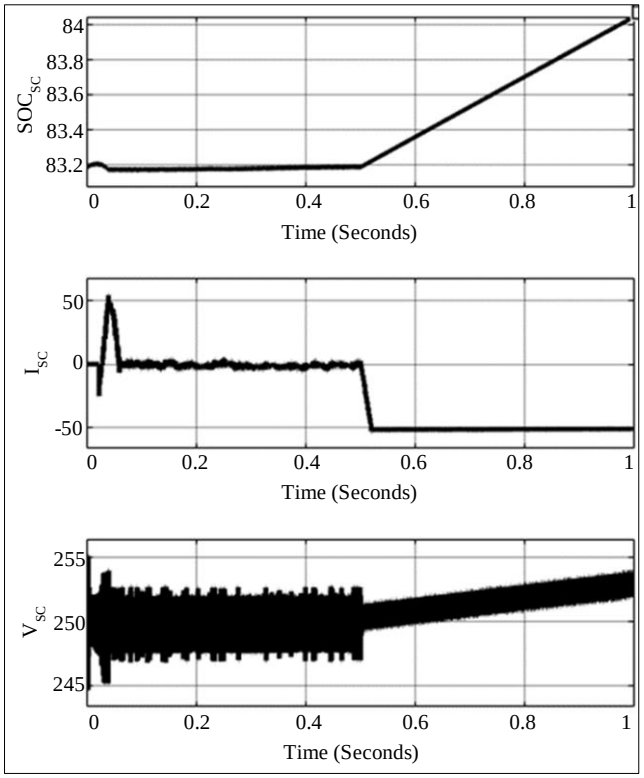

Fig. 12 SC characteristics for model (ii)

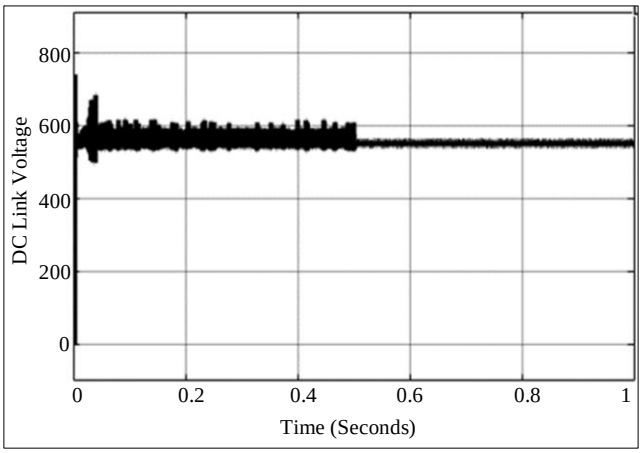

Fig. 13 DC bus voltage for model (ii)

The model (ii) is updated with FIS at the voltage regulator of the battery module, creating a model (iii), which is run for the same operating modes as the PMSM. Figure 16 represents the fuzzy rule base of the 49 rules set in the FIS voltage regulator. The Ibat* value is generated as per the input variables E and CE. The battery SOC comparison graph with all the models (i), (ii), and (iii) is presented in Figure 17, showing a drop as per the discharge from the battery pack.

As per Figure 17, the slop of the SOC of model (i) is steeper as compared to models (ii) and (iii) SOCs. As the model is run with only a battery module, the discharge current is higher, and due to CV control, the current is also not limited. The comparison of currents of the battery pack for the three models is presented in Figure 18. As observed in Figure 18, the current magnitude and peak for model (i) are very high as compared to models (ii) and (iii). As the model (ii) and (iii) are operated with CC control in the battery module the currents are limited as per the voltage regulator limitations. For the same models, the DC bus voltage comparison graphs are also presented in Figure 19, which is measured at the input of the VSC.

As per Figure 19 the DC bus voltage ripple is seen to be lesser for the model with FIS voltage regulator in the battery module. This shows a significant improvement in the performance of the proposed topology with SC module support and FIS based voltage regulator. A parametric comparative table with an analysis of the signals is presented in Table 3 to determine the robust topology.

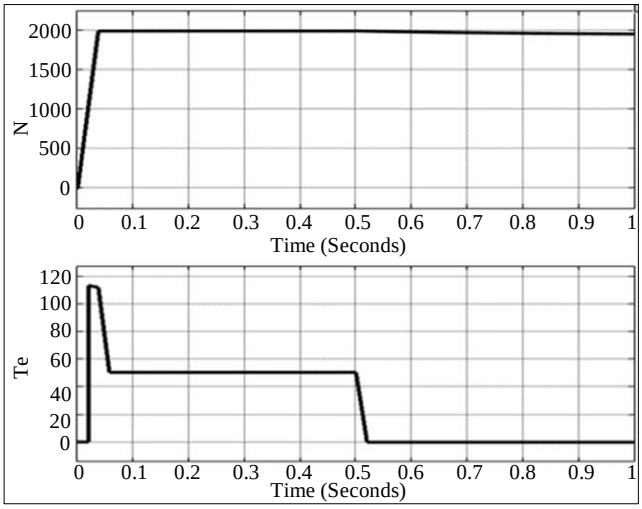

Fig. 14 Stator currents (ISabc) and mechanical torque (Tm) for model (ii).

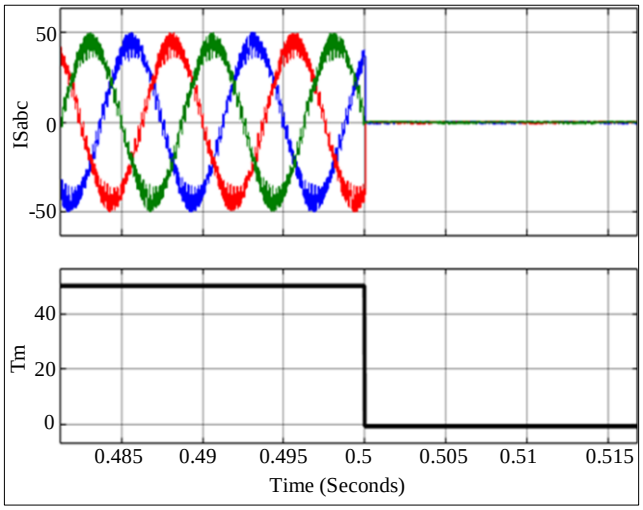

Fig. 15 PMSM speed (N) and electro-magnetic torque (Te) of model (ii)

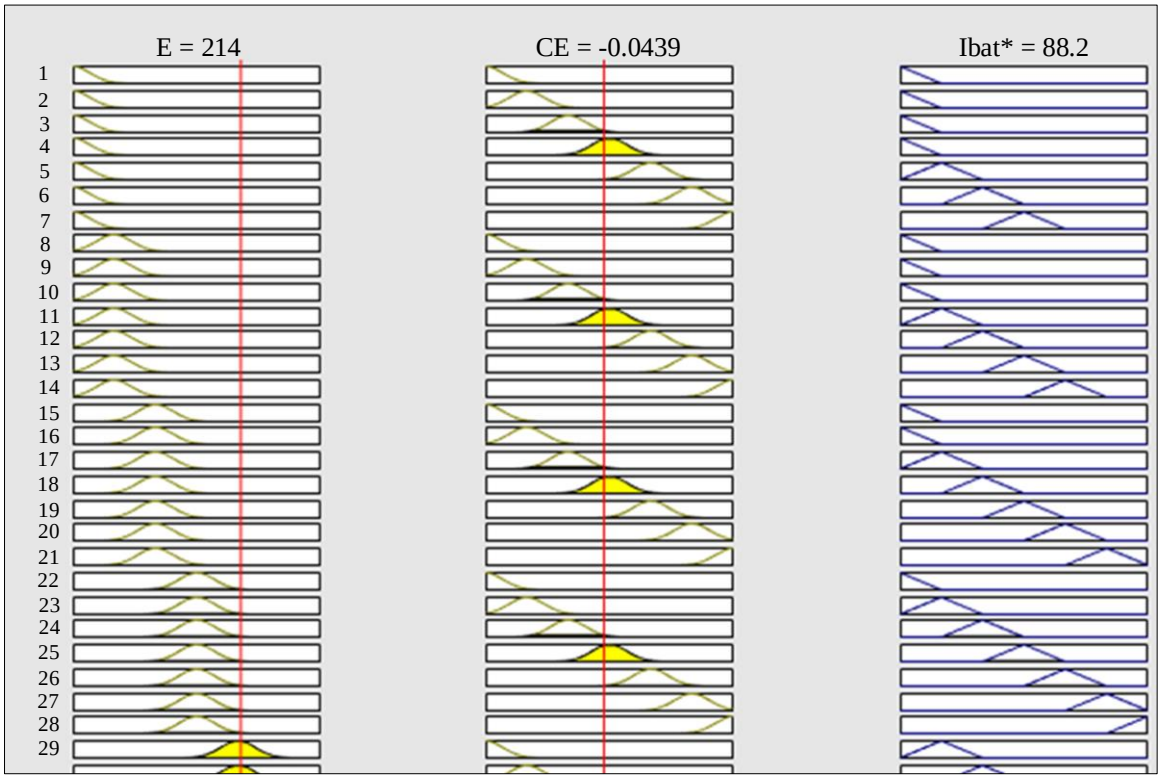

Fig. 16 FIS rules

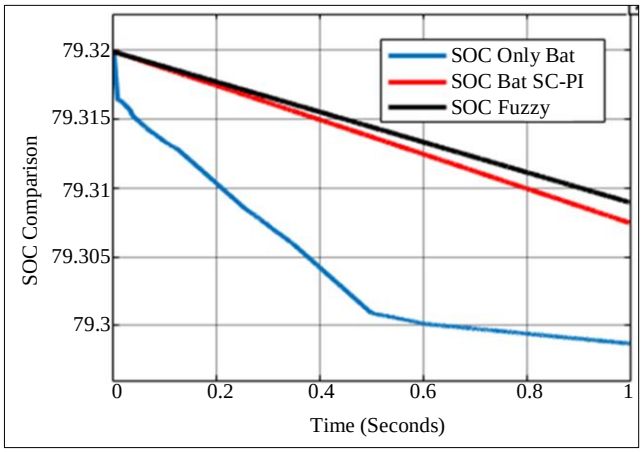

Fig. 17 Battery pack SOC comparison for models (i), (ii), and (iii)

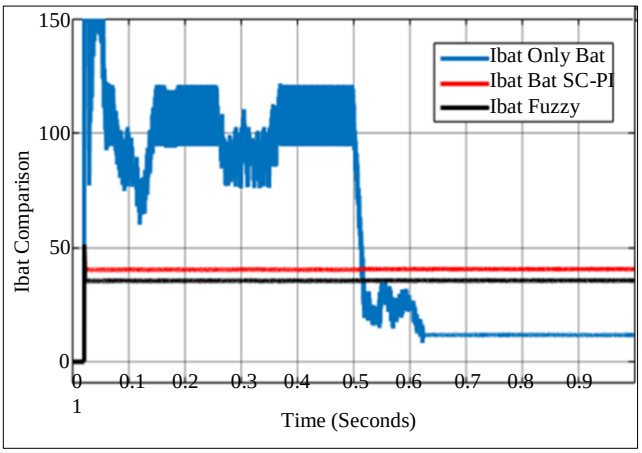

Fig. 18 Battery pack current comparison for models (i), (ii), and (iii)

Table 3. Comparative parameters

Name of the Parameter	Model (i) (Only Battery as a Source)	Model (ii) (Battery +Supercapacitor as a Source with PI Controller)	Model (iii) (Battery +Supercapacitor as a Source with Fuzzy Controller)
Ibat	100A	40A	35A
Ibat Initial Peak	600A	55A	50A
Vdc	560V	560V	560V
Vdc Ripple	12.7%	8.6%	5.3%
Vdc Peak	900V	680V	650V
SOC of Battery in %	79.206	79.305	79.309

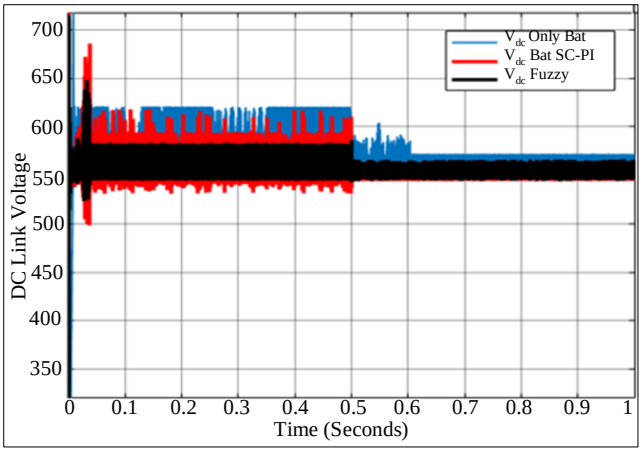

Fig. 19 DC bus voltage comparison for models (i), (ii), and (iii)

5. Conclusion

This paper presents an analysis of the internal structure of the EV driving circuit topology. The analysis includes detailed modelling and discussions accompanied by graphs. The configuration of each module of the circuit, including the battery, SC, and PMSM circuits and controllers, is described with detailed mathematical expressions.

The analysis compares the performance of the circuit with only the battery connected to PMSM and with the battery and SC connected. The battery and SC module are updated with a FIS regulator, replacing the conventional PI regulator, to improve the parameters of the battery module. According to the comparison Table 3, it is determined that the topology with SC and FIS voltage regulators is more stable, with reduced peak value generation.

There is a noticeable drop in the peak value of the battery current and ripple of the DC bus voltage for the SC and FIS integrated topology. This enhances the battery's health and reliability, thereby increasing the durability of the circuit for higher rated EVs.

References

[1] Krishna Veer Singh, Hari Om Bansal, and Dheerendra Singh, "A Comprehensive Review on Hybrid Electric Vehicles: Architectures and Components," *Journal of Modern Transportation*, vol. 27, pp. 77-107, 2019. [CrossRef] [Google Scholar] [Publisher Link]

[2] Priti Dinkar Dhigare, and Sanjay D. Yadav, "A Review of Hybrid Electric Vehicle: A Trend and Advanced Technologies," *International Journal of Research in Engineering and Technology*, vol. 7, no. 5, pp. 7128-7134, 2020. [Publisher Link]

[3] A. Loganayaki, and R. Bharani Kumar, "Permanent Magnet Synchronous Motor for Electric Vehicle Applications," *5th International Conference on Advanced Computing & Communication Systems (ICACCS)*, India, pp. 1064-1069, 2019. [CrossRef] [Google Scholar] [Publisher Link]

[4] Muhammad Usman Sardar et al., "Permanent Magnet Synchronous Machine Control Performance and Analysis for Environment-Friendly Electric Vehicle Applications," *Engineering Procedings*, vol. 46, no. 1, 2023. [CrossRef] [Google Scholar] [Publisher Link]

[5] Michele Pipicelli et al., "Assessment of Battery-Supercapacitor Topologies of an Electric Vehicle under Real Driving Conditions," *Vehicles*, vol. 5, no. 2, pp. 424-445, 2023. [CrossRef] [Google Scholar] [Publisher Link]

[6] Idris Azizi, and Hammoud Rajeai, "A New Strategy for Battery and Supercapacitor Energy Management for an Urban Electric Vehicle," *Electrical Engineering*, vol. 100, pp. 667-676, 2018. [CrossRef] [Google Scholar] [Publisher Link]

[7] Li Bao, Lingling Fan, and Zhixin Miao, "Real-Time Simulation of Electric Vehicle Battery Charging Systems," *North American Power Symposium (NAPS)*, USA, pp. 1-6, 2018. [CrossRef] [Google Scholar] [Publisher Link]

[8] P. Ramesh et al., "Development of a PMSM Motor Field-Oriented Control Algorithm for Electrical Vehicles," *Materials Today: Proceedings*, vol. 65, Part 1, pp. 176-187, 2022. [CrossRef] [Google Scholar] [Publisher Link]

[9] Qiao Zhang, and Weiwen Deng, "An Adaptive Energy Management System for Electric Vehicles Based on Driving Cycle Identification and Wavelet Transform," *Energies*, vol. 9, no. 5, 2016. [CrossRef] [Google Scholar] [Publisher Link]

[10] Xizheng Zhang et al., "L2-Gain Adaptive Robust Control for Hybrid Energy Storage System in Electric Vehicles," *IEEE Transactions on Power Electronics*, vol. 36, no. 6, pp. 7319-7332, 2021. [CrossRef] [Google Scholar] [Publisher Link]

[11] Zhangyu Lu, and Xizheng Zhang, "Composite Non-Linear Control of Hybrid Energy-Storage System in Electric Vehicle," *Energies*, vol. 15, no. 4, 2022. [CrossRef] [Google Scholar] [Publisher Link]

[12] Sungchul Jung, and Jongsun Ko, "Study on Regenerative Energy Recovery of Electric Vehicle through Voltage Control Using Switched Capacitor," *IEEE Transactions on Vehicular Technology*, vol. 70, no. 5, pp. 4324-4339, 2021. [CrossRef] [Google Scholar] [Publisher Link]

[13] Shoeib Heydarie et al., "Maximizing Regenerative Braking Energy Recovery of Electric Vehicles through Dynamic Low-Speed Cutoff Point Detection," *IEEE Transactions on Transportation Electrification*, vol. 5, no. 1, pp. 262-270, 2019. [CrossRef] [Google Scholar] [Publisher Link]

[14] Andrei Oprea, and Dan Floricau, "Field Oriented Control of Permanent Magnet Synchronous Motor with Graphical User Interface," *12th International Symposium on Advanced Topics in Electrical Engineering (ATEE)*, Romania, pp. 1-4, 2021. [CrossRef] [Google Scholar] [Publisher Link]

[15] E. Yesilbag, and L.T. Ergene, "Field Oriented Control of Permanent Magnet Synchronous Motors Used in Washers," *16th International Power Electronics and Motion Control Conference and Exposition*, Turkey, pp. 1259-1264, 2014. [CrossRef] [Google Scholar] [Publisher Link]

[16] Liu Zheng, and Fan Shao-sheng, "An Intelligent Charging Control Method for Electric Vehicle Charging System," *IEEE 2nd Annual Southern Power Electronics Conference (SPEC)*, New Zealand, pp. 1-6, 2016. [CrossRef] [Google Scholar] [Publisher Link]

[17] Salman Habib et al., "A Comprehensive Study of Implemented International Standards, Technical Challenges, Impacts and Prospects for Electric Vehicles," *IEEE Access*, vol. 6, pp. 13866-13890, 2018. [CrossRef] [Google Scholar] [Publisher Link]

[18] Jiang-Hua Lu et al., "Research on Seamless Transfer from CC to CV Modes for IPT EV Charging System Based on Double-Sided LCC Compensation Network," *IEEE Energy Conversion Congress and Exposition (ECCE)*, USA, pp. 1-6, 2016. [CrossRef] [Google Scholar] [Publisher Link]

[19] Abd El Halim et al., "Grid-Connected EV Fast Charging Stations Using Vector Control and CC-CV Techniques," *European Journal of Automated Systems*, vol. 56, no. 6, pp. 993-1001, 2023. [CrossRef] [Google Scholar] [Publisher Link]

[20] A.A. Eajal et al., "Fuzzy Logic-Based Charging Strategy for Electric Vehicles Plugged into A Smart Grid," *International Journal of Process Systems Engineering*, vol. 4, no. 2-3, pp 119-137, 2017. [CrossRef] [Google Scholar] [Publisher Link]

[21] G. Madhuri et al., "Fast Charging Electric Vehicle Using Fuzzy Logic Controller," *International Journal of Engineering Research & Technology*, vol. 9, no. 5, pp. 499-502, 2020. [Google Scholar] [Publisher Link]

[22] George Cristian Lazaroiu, and Mariacristina Roscia, "Fuzzy Logic Strategy for Priority Control of Electric Vehicle Charging," *IEEE Transactions on Intelligent Transportation Systems*, vol. 23, no. 10, pp. 19236-19245, 2022. [CrossRef] [Google Scholar] [Publisher Link]